

A Journal of the Gesellschaft Deutscher Chemiker

# Angewandte Chemie

GDCh

International Edition

www.angewandte.org

## Accepted Article

**Title:** Engineered Polymeric Carbon Nitride for Photocatalytic Diverse Functionalization of Electronic-Rich Alkenes

**Authors:** Youqing Yang, Jiwei Shi, Chenguang Liu, Qiong Liu, Jian Yang, Xiaogang Tong, Jiong Lu, and Jie Wu

This manuscript has been accepted after peer review and appears as an Accepted Article online prior to editing, proofing, and formal publication of the final Version of Record (VoR). The VoR will be published online in Early View as soon as possible and may be different to this Accepted Article as a result of editing. Readers should obtain the VoR from the journal website shown below when it is published to ensure accuracy of information. The authors are responsible for the content of this Accepted Article.

**To be cited as:** *Angew. Chem. Int. Ed.* **2024**, e202417099

**Link to VoR:** <https://doi.org/10.1002/anie.202417099>

# Engineered Polymeric Carbon Nitride for Photocatalytic Diverse Functionalization of Electronic-Rich Alkenes

Youqing Yang,<sup>‡[a,b]</sup> Jiwei Shi,<sup>‡[b,c]</sup> Chenguang Liu,<sup>[b]</sup> Qiong Liu,<sup>[b,d]</sup> Jian Yang,<sup>[b]</sup> Xiaogang Tong,<sup>\*,[b,e]</sup> Jiong Lu,<sup>\*,[b]</sup> and Jie Wu<sup>\*,[b]</sup>

**Abstract:** Engineered polymeric carbon nitride represents a promising class of metal-free semiconductor photocatalysts for organic synthesis. Herein, we utilized engineered polymeric carbon nitride nanosheets, which exhibit an increased specific surface area and bandgap due to enhanced quantum confinement from vacancy enrichment. These nanosheets serve as a heterogeneous organic semiconductor photocatalyst to facilitate diverse functionalizations of electron-rich alkenes, including arylsulfonylation, aminodifluoroalkylation, and oxytrifluoromethylation. This catalytic system operates under mild conditions, offering excellent functional group compatibility and high yields. Additionally, the catalyst demonstrates outstanding recyclability and efficiency in flow reactors, highlighting its significant potential for industrial applications.

## Introduction

In the past decade, visible-light photoredox catalysis has emerged as a powerful tool in synthetic chemistry, facilitating bond formations through unique reaction pathways and modes.<sup>[1]</sup> Moreover, most photoreactions offer advantages such as mild reaction conditions, minimal waste generation, and the utilization of clean energy source. However, concerns regarding the high cost and toxicity of conventional photocatalysts, such as Ir(III) and Ru(II) complexes, have prompted researchers to explore alternatives like earth-abundant transition metals, metal-free organic dyes, and other commercial materials.<sup>[2]</sup> Among these alternatives, heterogeneous materials have gained prominence for their ease of removal and recyclability, presenting a promising alternative over homogeneous catalysts in photocatalytic reactions.<sup>[3]</sup>

[a] Dr. Y. Yang

Key Laboratory of Green and Precise Synthetic Chemistry and Applications, Ministry of Education; Anhui Key Laboratory of Synthetic Chemistry and Applications, Huaibei Normal University, Huaibei, Anhui 235000, P.R. China

[b] Dr. Y. Yang, J. Shi, Dr. C. Liu, Dr. Q. Liu, Dr. J. Yang, Dr. X. Tong., Dr. J. Lu, Dr. J. Wu

Department of Chemistry, National University of Singapore, 3 Science Drive 3, Singapore 117543, Republic of Singapore  
E-mail: tongxg@ynu.edu.cn; chmluj@nus.edu.sg; chmjie@nus.edu.sg

[c] J. Shi

Tianjin University International Campus of Tianjin University Binhai New City, Fuzhou 350207, P. R. China

[d] Dr. Q. Liu

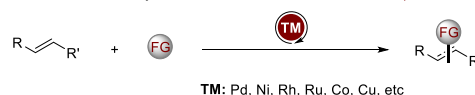
Institute of Analysis, Guangdong Academy of Sciences (China National Analytical Center, Guangzhou) 510070, P. R. China

[e] Dr. X. Tong

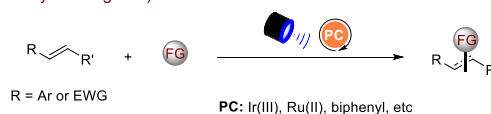
School of Chemical Science and Technology, Yunnan University, Kunming 650091, P. R. China

[‡] these authors contributed equally to this work.

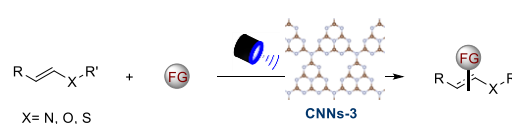
a. Transition-metal catalyzed functionalization of alkenes (well established)



b. Photo-induced functionalization of styrene and electron-deficient alkenes (widely investigated)



c. **This work:** Photocatalytic functionalization of electron-rich alkenes via CNNs-3 (rarely studied)



### Challenges

- Transformation with electron-rich alkenes selectively
- Light penetration in heterogeneous solid-liquid reaction mixtures

✓ high efficiency ✓ good functional group compatibility ✓ high recyclability

**Scheme 1.** (a) Transition-metal catalyzed functionalization of alkenes. (b) Photo-induced functionalization of styrene and electron-deficient alkenes. (c) This work: the utilization of CNNs-3 as heterogeneous photocatalyst for diverse functionalization of electron-rich alkenes.

Polymeric carbon nitride (PCN), composed mainly of carbon and nitrogen atoms in a graphitic structure, can be readily prepared from cost-effective and readily available bulk chemicals like melamine and cyanuric acid.<sup>[4]</sup> By modulating their properties, such as vacancy engineering, doping, and structure engineering, PCN has become one of the most appealing materials for heterogeneous photocatalysis.<sup>[5]</sup> Notably, PCN nanosheets (CNNs), characterized with a large specific surface area and the presence of vacancies, have demonstrated promising photocatalytic efficiency.<sup>[6]</sup> In 2021, we developed two types of heteroatom-doped PCN nanosheets (SCN-V and BSCN-V) by integrating nanostructure construction, heteroatom doping, and vacancy engineering into one hybrid platform, thereby demonstrating superior photocatalytic activities in a variety of organic photochemical transformations, such as defluoroborylation, [2+2] cycloaddition, C–N, C–S, C–O cross-couplings, and regioselective hydrosilylation.<sup>[7]</sup> On the other hand, PCN's successful application in continuous flow platform has overcome the challenge of limited light penetration in heterogeneous solid-liquid reaction mixtures, rendering it suitable for industrial applications.<sup>[8]</sup> Therefore, PCN's merits prompted us to further improve their capabilities and explore their application to other types of photochemical reactions.

The functionalization of alkenes has significantly enriched the toolkit of complex organic molecules in medicinal and materials science.<sup>[9]</sup> Compared to the conventional transition-metal catalysis (Scheme 1a),<sup>[10]</sup> photocatalysis has emerged as an efficient and sustainable strategy for alkene functionalization in

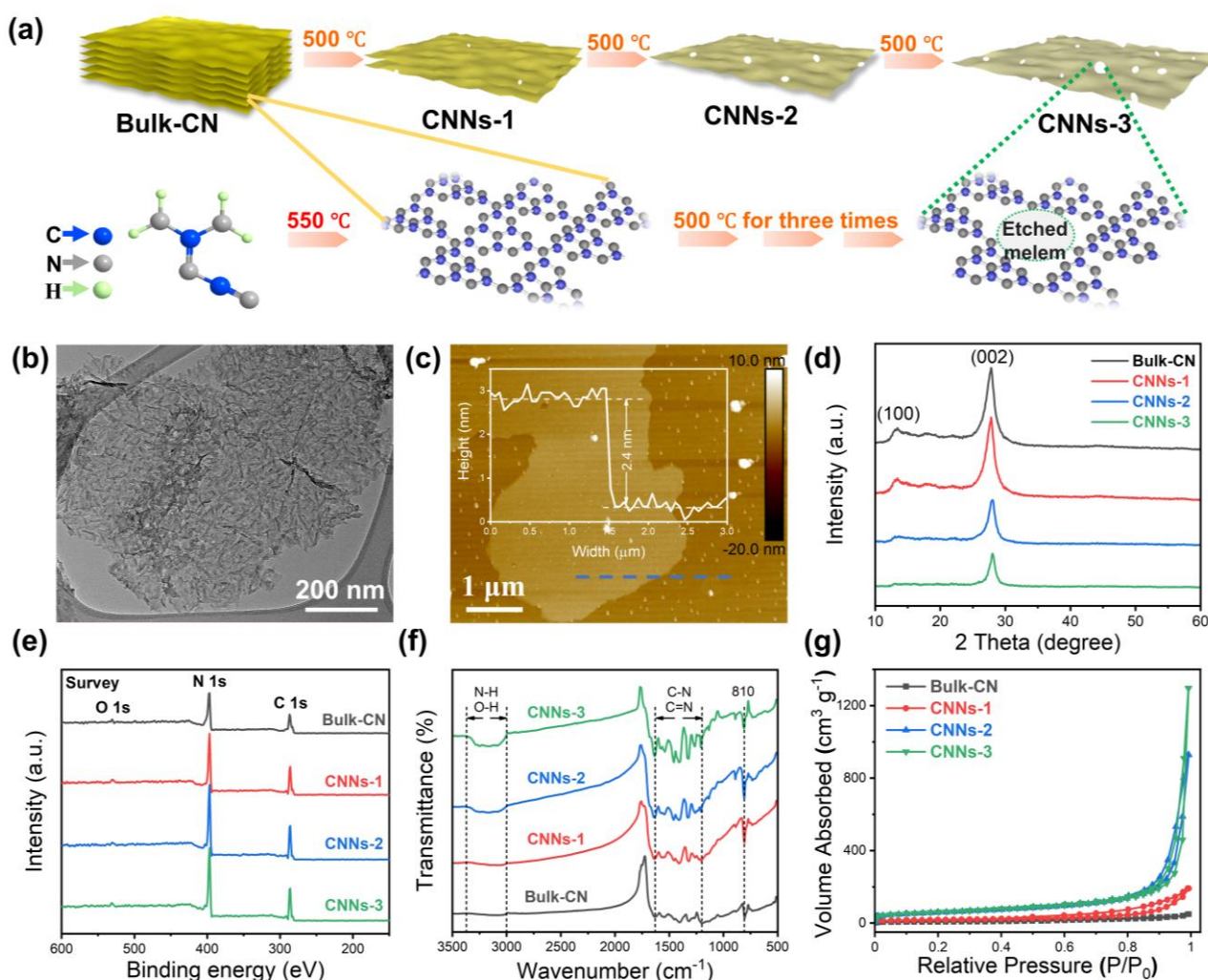


**Figure 1.** (a) Procedure of preparing CNNs. (b) TEM of CNNs-3. (c) AFM of CNNs-3 with height profile inset. (d) XRD of CNNs. (e) XPS survey spectra of CNNs. The peaks at 286 eV, 397 eV, and 530 eV belong to the C 1s, N 1s, and O 1s regions, respectively. (f) FTIR of Bulk-CN, CNNs-1, CNNs-2 and CNNs-3. The peak at 810  $\text{cm}^{-1}$  is attributed to the bending vibrations of the heptazine ring, the peaks in the 1200 to 1600  $\text{cm}^{-1}$  range correspond to C-N and C=N bonds. The broad peak in the 3000–3300  $\text{cm}^{-1}$  region is associated with N-H and O-H bonds. (g) BET surface areas of CNNs.

recent years.<sup>[11]</sup> However, the main focus of these transformations is currently on styrene and electron-deficient alkenes (Scheme 1b).<sup>[12]</sup> The photocatalyzed functionalization of electron-rich alkenes containing oxygen, nitrogen, or sulfur atoms remains underexplored.<sup>[13]</sup> This is largely due to the profound electronegativity and the repulsion effect from their lone-pair electrons of these heteroatoms, which significantly reduce their reactivity and selectivity.<sup>[14]</sup> Pioneer work has been achieved by Barton and colleagues in 1994, yielding selenoethers with excellent yield and regioselectivity from S-phenyl selenosulfonates and vinyl ethers by using  $\text{Ru}(\text{bpy})_3^{2+}$ /visible-light system.<sup>[15]</sup> In 2018, Yoshimi and co-workers documented a photoinduced redox system using biphenyl (BP) and 1,4-dicyanonaphthalene (DCN) as an

organic photocatalyst for the preparation of cross-coupling adducts between electronically-differentiated donor and acceptor alkenes containing a nucleophile under mild conditions.<sup>[16]</sup> More recently, Glorius and co-workers disclosed a base-controlled strategy toward the reincorporation/release of  $\text{SO}_2$  in photocatalyzed radical difunctionalization of alkenes.<sup>[17]</sup> In addition to vinyl ethers, the photocatalyzed difunctionalization of enamides and enecarbamate have been reported by Studer,<sup>[18]</sup> Fu,<sup>[19]</sup> Li,<sup>[20]</sup> and other groups,<sup>[21]</sup> enabling the synthesis of  $\alpha,\beta$ -substituted amines through oxyalkylation and oxy-/amino-carbotrifluoromethylation. Despite these progresses, the pursuit of more straightforward and environmental-friendly strategies for the functionalization of electron-rich alkenes is of high synthetic significance.

In this study, we present a straightforward and practical protocol for the functionalization of electron-rich alkenes using engineered ultra-thin CNNs as photocatalysts, including arylsulfonylation, aminodifluoroalkylation, and oxytrifluoromethylation (Scheme 1c). Moreover, the CNNs employed in these heterogeneous photocatalyzed reactions are easily prepared from inexpensive and readily available starting materials via several rounds of calcination under the air. Our approach demonstrates a high isolated yield and a broad substrate scope, offering a practical solution for functionalization of electron-rich alkenes.

## Results and Discussion

### Preparation and structure characterization of CNNs

Using inexpensive dicyandiamide as the precursor, we first synthesized the Bulk-CN and subsequently transformed it into three kinds of CNNs materials (CNNs-1, CNNs-2 and CNNs-3) through straightforward consecutive thermal exfoliation processes in air (Figures 1a and S1). Transmission electron microscopy (TEM) and scanning electron microscopy (SEM) images revealed the transformation of the bulk PCN to two-dimensional lamellar-like structures (Figures 1b, S2 and S3). Atomic force microscopy (AFM) image confirmed that the average thickness of CNNs-3 is approximately  $2.4 \pm 0.19$  nm (Figures 1c and S4), providing clear evidence of successful exfoliation to atomically thin nanosheets. The X-ray diffraction (XRD) patterns of CNNs closely resembled those of Bulk-CN, featuring two characteristic peaks at  $13.2^\circ$  and  $27.8^\circ$  corresponding to (100) and (002) crystal planes (Figures 1d and S5).<sup>[22]</sup> The peaks in the CNN exhibit slight shifts ((100) peak to a lower angle, (002) peak to a higher angle) and a reduction in intensity, attributed to the thermal "etching effect" causing the in-plane layer size to become smaller (observed in the (100) peak) and decreases in interlayer stacking due to the planarization of undulating single layers caused by heating (seen in the (002) peak).<sup>[23]</sup> X-ray photoelectron spectroscopy (XPS) measurements further revealed that the chemical states of carbon and nitrogen in CNNs-3 were identical to those in Bulk-CN, as evidenced by the absence of significant binding energy shifts in the core-level C1s and N1s spectra (Figures 1e and S6). Furthermore, the Fourier transform infrared (FT-IR) spectra indicate that the characteristic peaks of the C-N heterocycles contained in CNNs-3 and Bulk CN are almost identical (Figure 1f), revealing their similar chemical structures.<sup>[24]</sup> The typical vibrational mode of the melamine heptazine ring is observed at  $810\text{ cm}^{-1}$ , while the peaks in  $1200$  to  $1600\text{ cm}^{-1}$  region are attributed to the characteristic stretching modes of the C-N heterocycles. Multiple broad peaks in the  $3000$ - $3300\text{ cm}^{-1}$  are assigned to the stretching modes of N-H and O-H bonds, possibly because of the amino groups and surface-absorbed  $\text{H}_2\text{O}$  molecules.<sup>[25]</sup> It is worth noting that all peaks of CNNs-3 are sharper than those of BCN, which is due to the more ordered stacking of hydrogen-bond cohered long strands of polymeric melon units that survive thermal exfoliation.<sup>[24]</sup> Additionally, the Brunauer-Emmett-Teller (BET) specific surface area of CNNs also enhances with increasing thermal exfoliation (Figure 1g). Notably, the specific

surface area of CNNs-3 is calculated to be  $178.9\text{ m}^2\text{ g}^{-1}$ , which is approximately 29 times larger than that of Bulk-CN ( $6.1\text{ m}^2\text{ g}^{-1}$ ), which could provide numerous active sites for surface adsorption and activation of reactive species, facilitating photocatalytic interfacial reactions.<sup>[26]</sup> Overall, all CNNs

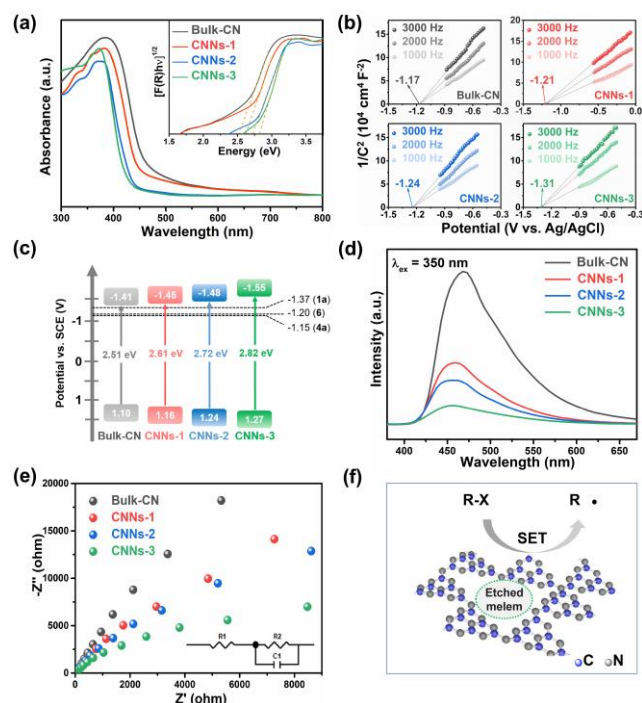


**Figure 2.** (a) UV-Vis spectra of CNNs. (b) Mott-Schottky plots of CNNs. (c) Band gap of CNNs. (d) Steady state PL spectra of CNNs. (e) EIS Nyquist plots of CNNs. (f) Designed reaction model.

maintain a similar crystal structure to bulk carbon nitride but exhibit distinctive surface properties with significantly larger specific surface area. These characteristics may enhance their catalytic performance, rendering them to possess efficient catalytic activity for various photocatalytic reactions.

### Optical properties and band structures of CNNs

The optical absorption characteristics of all CNNs were investigated using ultraviolet-visible diffuse reflectance spectroscopy (UV-vis DRS), and the bandgap energies were determined through the Kubelk-Munk method.<sup>[27]</sup> In comparison to Bulk-CN, CNNs exhibited a blue-shifted absorption edge, signifying an enlarged bandgap. This is presumably due to the strong quantum confinement effect of the formed ultrathin nanosheet structure, which causes the edges of the conduction and valence bands to shift in the opposite direction (Figure 2a).<sup>[24]</sup> Specifically, the thermal exfoliation gradually increases the bandgap of Bulk-CN (2.51 eV) to that of CNNs-3 (2.82 eV). The valence band XPS spectra further corroborated this result, showing a significant increase in the valence band maximum from Bulk-CN to CNNs-3 (Figure S11).<sup>[28]</sup>

The flat band potentials were estimated from the intercept of the extrapolated lines in Mott-Schottky (M-S) plots (Figure 2b), with CNNs-3 displaying the highest potential among the samples ( $-1.17$ ,  $-1.21$ ,  $-1.24$ , and  $-1.31$  V (vs. Ag/AgCl) for Bulk-CN, CNNs-1, CNNs-2, and CNNs-3, respectively). Moreover,

the positive slopes indicating an n-type semiconducting character for all CNNs samples. As the conduction band potential ( $E_{CB}$ ) of n-type semiconductors is generally higher than the flat band potential by approximately 0.2 V, the  $E_{CB}$  are estimated to be -1.41, -1.45, -1.48 and -1.55 eV (vs. SCE) for Bulk-CN, CNNs-1, CNNs-2, and CNNs-3, respectively (Figure 2c).<sup>[29]</sup>

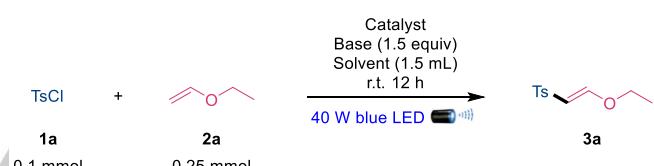
Additionally, the increasing bandgap from Bulk-CN to CNNs-3 was corroborated with the blue shift in the photoluminescence (PL) spectrum (from 468 nm to 455 nm, Figure 2d). The decreasing PL intensity indicates enhanced electron-hole separation efficiency across the CNNs, leading to lower recombination rate of electrons and holes, consequently increasing the photocatalytic activity.<sup>[30]</sup> The separation efficiency of electron-hole pairs was further revealed through time-resolved photoluminescence (TRPL) spectroscopy, surface photovoltage (SPV) spectroscopy, and transient photocurrent density measurements. The average fluorescence lifetime of CNNs-3, calculated from the TRPL spectra (Figure S7), was found to be 11.7 ns, shorter than that of bulk-CN (15.3 ns), CNNs-1 (14.5 ns), and CNNs-2 (13.6 ns). These results demonstrate the efficient charge transfer in photocatalytic reactions.<sup>[31]</sup> A distinct positive SPV response was observed for the different materials within the 300–450 nm range (Figure S8), which is a characteristic of n-type semiconductors.<sup>[28]</sup> This SPV response indicates that, with progressive thermal exfoliation, the response intensity gradually increases, confirming that CNNs-3 is the most effective in separating photogenerated electron-hole pairs. Compared to bulk-CN, CNNs-1, and CNNs-2, CNNs-3 exhibited the highest photocurrent, indicating the most efficient charge separation under light irradiation. The lower recombination and charge transfer rate over CNNs were also supported by electrochemical impedance spectroscopy (EIS) Nyquist plots, where the diameter of CNNs-3 is dramatically reduced compared to Bulk-CN (Figure 2e).<sup>[27]</sup> Lastly, the efficient charge transfer rate was further verified by the enhancement of the electron spin resonance (ESR) signal at  $g=2.0$  over CNNs-3 (Figure S13), further corroborates the enhanced charge transfer rate in vacancy-rich CNNs. This is verified by the gradually enhanced ESR intensity along with the enhanced vacancy concentration within CNNs.<sup>[32]</sup> Taking all the above results, CNNs-3 exhibits the greatest separation ability for electron-hole pairs among the CNNs, where the excited electrons can be efficiently transferred to target molecules that absorbed on the surface. This distinct capability could be harnessed for generating radicals via single electron transfer (SET), offering intriguing possibilities for organic chemistry applications (Figure 2f).

### Investigation of reaction conditions

With different PCNs prepared, our investigation commenced with the arylsulfonylation of electron-rich alkenes, using tosyl chloride (**1a**) and ethyl vinyl ether (**2a**) as the model substrates under an argon atmosphere in MeCN and irradiated with 456 nm LED light (40 W) at room temperature for 12 h (Table 1). 5 mg of PCN were used for the screening, and improved yield of desired product **3a** from 39% to 94% was obtained with increasing etchings from Bulk-CN to CNNs-3 (entries 1-4). Furthermore, the catalytic performance of CNNs-3 surpassed well-established homogeneous and heterogeneous catalysts,

such as  $g\text{-C}_3\text{N}_4$ , mpg- $\text{C}_3\text{N}_4$ , K-PHI,  $\text{Ir}(\text{ppy})_2(\text{dtbbpy})\text{PF}_6$ , and  $\text{Ru}(\text{bpy})_3(\text{PF}_6)_2$  (entries 5-9). The superior performance of CNNs-3 over other carbon nitride forms could be attributed to its distinct advantages, including an outstanding specific surface area (178.9  $\text{m}^2/\text{g}$ ) and pore volume (1.97  $\text{m}^3/\text{g}$ ), ultrathin nanosheets with a porous architecture, and enhanced charge separation at the reactive sites (bandgap, 2.82 eV). Further evaluation of various bases identified LiOH as the optimal choice (Table S3). Intriguingly, the absence of LiOH led to the detection of only 5% of the product, underscoring the indispensable role of the base (Table 1, entry 10). The choice of solvent also proved to be crucial, with dioxane yielding a modest 38% yield (entry 11). Notably, control experiments conducted in the absence of light exhibited no transformation, confirming its photoinduced nature (entry 12).

**Table 1. Optimization of arylsulfonylation of electron-rich alkenes<sup>a</sup>**



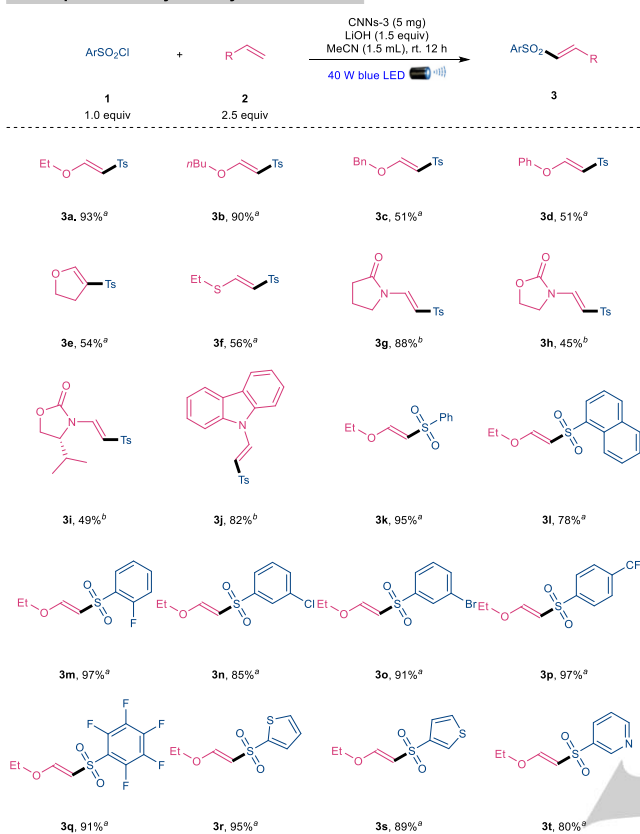
Entry	Catalyst (mg)	Base	Solvent	Yield (%) <sup>b</sup>
1	Bulk-CN (5)	LiOH	MeCN	39
2	CNNs-1 (5)	LiOH	MeCN	58
3	CNNs-2 (5)	LiOH	MeCN	68
4	<b>CNNs-3 (5)</b>	<b>LiOH</b>	<b>MeCN</b>	<b>94 (93)<sup>c</sup></b>
5	$g\text{-C}_3\text{N}_4$ (5)	LiOH	MeCN	44
6	mpg- $\text{C}_3\text{N}_4$ (5)	LiOH	MeCN	68
7	K-PHI (5)	LiOH	MeCN	61
8	$\text{Ir}(\text{ppy})_2(\text{dtbbpy})\text{PF}_6$ (1.8)	LiOH	MeCN	5
9	$\text{Ru}(\text{bpy})_3(\text{PF}_6)_2$ (1.7)	LiOH	MeCN	30
10	CNNs-3 (5)	--	MeCN	5
11	CNNs-3 (5)	LiOH	Dioxane	38
12 <sup>d</sup>	CNNs-3 (5)	LiOH	MeCN	0

Reaction conditions: <sup>a</sup>**1a** (0.1 mmol), **2a** (0.25 mmol), catalyst and LiOH (1.5 equiv.) in 1.5 mL MeCN under 456 nm LED light (40 W) at room temperature under argon for 12 h. <sup>b</sup>Yields were determined by <sup>1</sup>H NMR spectroscopy with  $\text{CH}_2\text{Br}_2$  as an internal standard. <sup>c</sup>Isolated yield. <sup>d</sup>The reaction was conducted in dark.

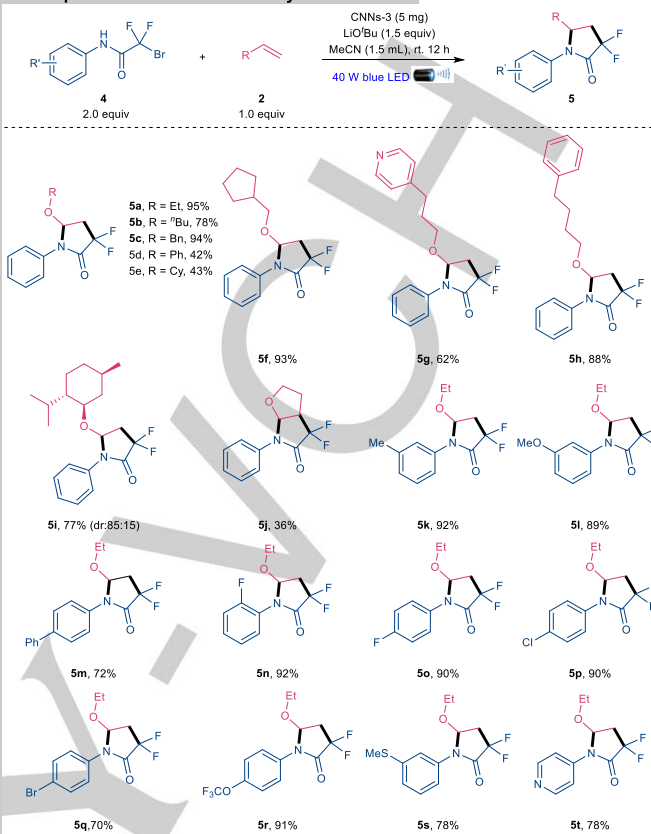
### Scope for the arylsulfonylation reaction

Under the optimal reaction conditions (Table 1, entry 4), we embarked on investigation of the substrate scope for the arylsulfonylation reaction, encompassing a diverse array of electron-rich alkenes and arylsulfonyl chlorides (Table 2a). A wide range of alkenes, including vinyl ethers (**2a**, **2b**, **2c**, **2d**), 2,3-dihydrofuran (**2e**), ethyl(vinyl)sulfane (**2f**), *N*-vinyl amides (**2g**, **2h**, **2i**), and 9-vinyl-9*H*-carbazole (**2j**), were suitable substrates in this protocol, yielding products **3a-3j** in 49-93%

## a. Scope for the arylsulfonylation reaction



## b. Scope for the aminodifluoroalkylation reaction



## c. Scope for the oxytrifluoromethylation reaction

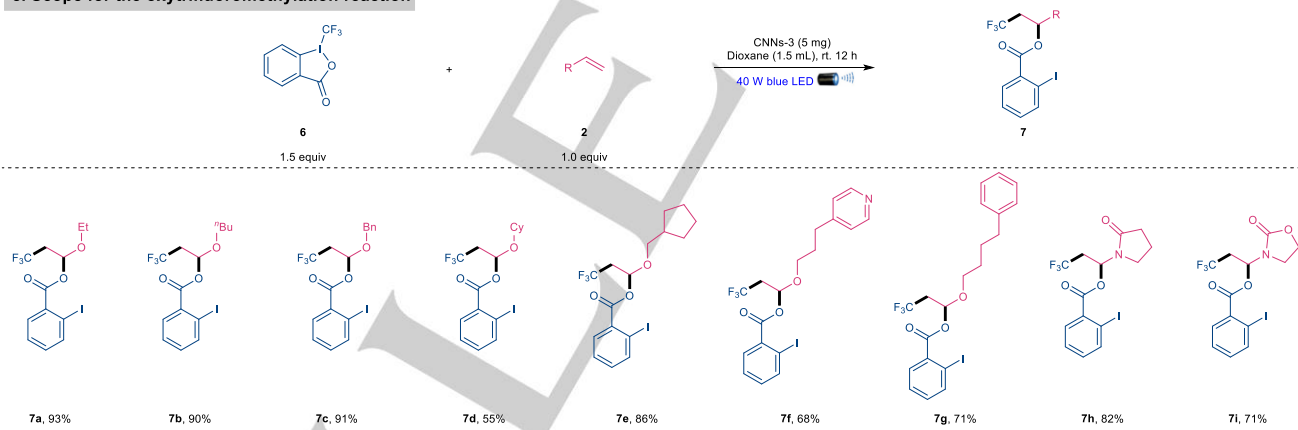
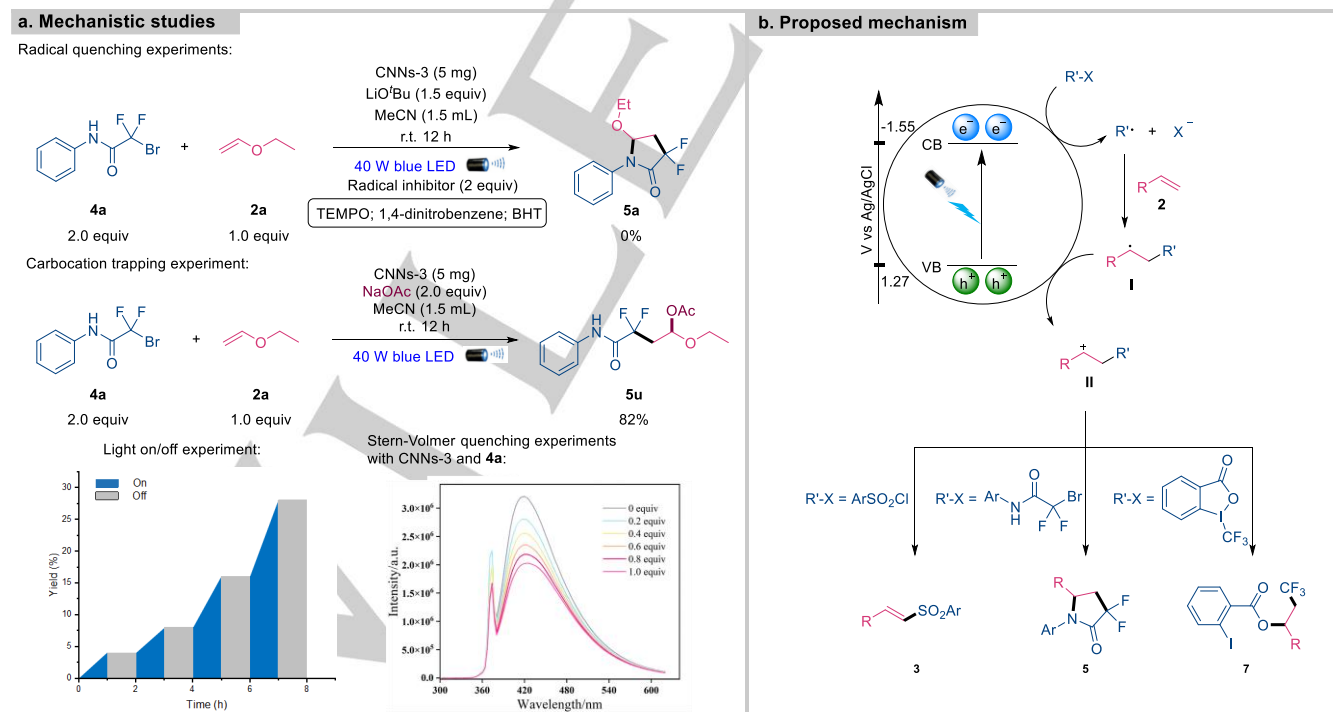
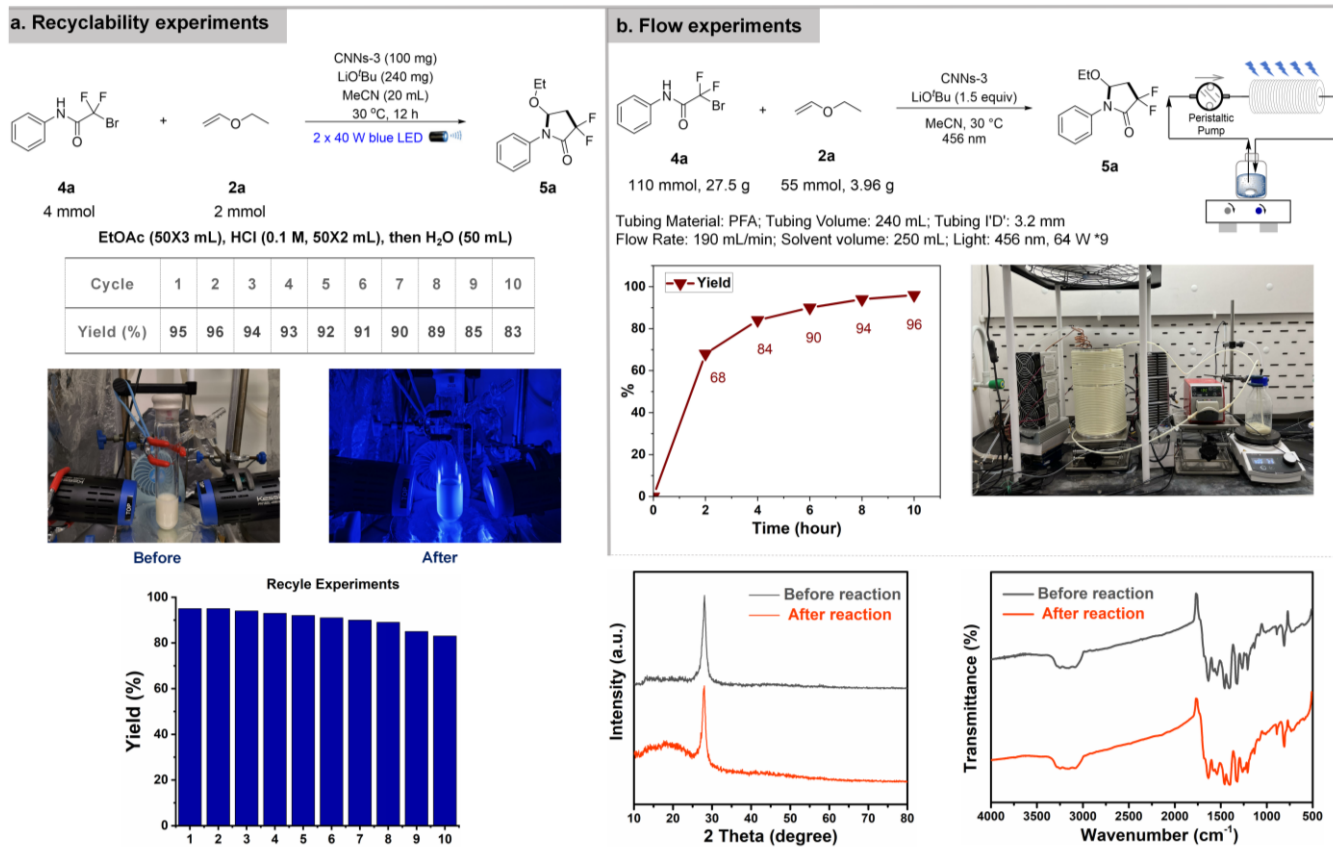


**Table 2. Scope for the arylsulfonylation reaction.** <sup>a</sup>1 (0.1 mmol), 2 (0.25 mmol), CNNS-3 (5 mg) and LiOH (1.5 equiv.) in 1.5 mL MeCN, irradiated by 456 nm LED light at room temperature under Ar for 12 h. <sup>b</sup>1 (0.1 mmol), 2 (0.25 mmol), CNNS-3 (5 mg) and K<sub>3</sub>PO<sub>4</sub> (1.5 equiv.) in 1.5 mL MeCN, irradiated by 456 nm LED light at room temperature under argon for 12 h. **Scope for the aminodifluoroalkylation reaction.** 2 (0.1 mmol), 4 (0.2 mmol), CNNS-3 (5 mg) and LiO<sup>t</sup>Bu (1.5 equiv.) in 1.5 mL MeCN, irradiated by 456 nm LED light at room temperature under Ar for 12 h. **Scope for the oxytrifluoromethylation reaction.** 2 (0.1 mmol), 6 (0.15 mmol), CNNS-3 (5 mg) in 1.5 mL dioxane, irradiated by 456 nm LED light at room temperature under argon for 12 h.

yield. Specially, minor adjustment of base in reaction conditions for the *N*-vinyl substrates (**2g-2j**) was performed, changing to K<sub>3</sub>PO<sub>4</sub> from LiOH. Aside from tosyl chloride, a range of aryl and heteroarylsulfonyl chlorides were viable substrates in this protocol. Notably, benzenesulfonyl chloride afforded product **3k** with an exceptional yield of 95%. Bulkier substrate like naphthalene-1-sulfonyl chloride also led to

product **3l** in a commendable 78% yield. Diverse electron withdrawing group, such as *ortho*-fluoro (**3m**), *meta*-chloro (**3n**), *meta*-bromo (**3o**), *para*-trifluoromethyl (**3p**), and perfluorophenyl (**3q**), could be introduced on the phenyl moiety of arylsulfonyl chlorides without a substantial impact on the reaction efficiency, affording the corresponding products in generally high yields (85-97%). Additionally,



various heteroaryl sulfonyl chlorides, such as *ortho*-thienyl (**3r**), *meta*-thienyl (**3s**), and *meta*-pyridyl (**3t**), participated smoothly in the reaction, delivering the corresponding products with good to excellent yields (80-95%).

### Scope for the aminodifluoroalkylation reaction

In a continued effort to showcase the versatile utility of CNNs-3 as a photocatalyst for electron rich alkene functionalization, we extended our investigation to the aminodifluoroalkylation reaction by using 2-bromo-2,2-difluoro-*N*-arylacetamide (**4**) as the partner and LiO<sup>t</sup>Bu as the base (Table S6). Our exploration of the substrate scope for the aminodifluoroalkylation reaction is outlined in Table 2b. A series of vinyl ethers were proved amenable, providing corresponding products (**5a-i**) in the range of 42-95% with 2-bromo-2,2-difluoro-*N*-phenylacetamide substrate. Notably, this method could furnish bicyclic lactam (**5j**) by using 2,3-dihydrofuran as the alkene substrate, albeit with a modest yield (36%). Next, the scope of 2-bromo-2,2-difluoro-*N*-arylacetamide partner was also examined with ethyl vinyl ether (**2a**) under standard conditions. The methodology facilitated the synthesis of diverse  $\alpha,\alpha$ -difluoro- $\gamma$ -lactam products with *N*-aryl bromodifluoroacetamides **4** bearing diverse substitution patterns and functional groups on the aryl scaffolds, such as *meta*-methyl (**5k**), *meta*-methoxy (**5l**), *para*-phenyl (**5m**), *para*-trifluoromethoxy (**5r**), and *meta*-methylthio (**5s**), affording in good to excellent yields (78-92%). Notably, this method could lead to the incorporation of halogens, resulting in the synthesis of  $\alpha,\alpha$ -difluoro- $\gamma$ -lactams bearing *ortho*-fluoro (**5n**), *para*-fluoro (**5o**), *para*-chloro (**5p**), and *para*-bromo (**5q**) substituents, with yields ranging from 70% to 92%. Corresponding products bearing chloro- and bromo- substituents are valuable, due to their great potential downstream functionalization via subsequent cross-coupling transformations. Furthermore, the method accommodated more intricate structures, resulting in the *para*-pyridyl products in good yield (**5t**).

### Scope for the oxytrifluoromethylation reaction

We further ventured into the trifluoromethylation reaction – a prominent area in organic chemistry – to enable efficient addition of trifluoromethyl groups to electron-rich alkenes. Despite the progress made with copper-based catalysts and photocatalysis, the heterogeneous catalysis is rarely studied.<sup>[33]</sup> Leveraging the efficiency of CNNs-3, we successfully accomplished the oxytrifluoromethylation of electron-rich alkenes using Togni reagent with high chemical selectivity (Table S7). The scope of various alkene substrates for oxytrifluoromethylation was examined (Table 2c). Specifically, various vinyl ethers were feasible in this protocol, yielding products (**7a-7g**) with 55-93% yields. Encouraged by these outcomes, we extended the evaluation to other alkene types with *N*-vinyl amides moiety. Notably, this oxytrifluoromethylation protocol led to the corresponding products **7h** and **7i** in good yields, suggesting that the methodology holds promise for the preparation of trifluoromethyl amides.

To demonstrate the practicality of our protocol with CNNs-3 as photocatalyst, we evaluated the scalability of the amino difluoroalkylation reaction under standard conditions (Figure 3a). First, the reaction was readily scaled-up to 2 mmol of **2a** without compromising its efficiency. Moreover, CNNs-3 catalyst was

recovered and reused for another reaction to investigate its recyclability. Remarkably, after ten reaction cycles, the catalytic activity remained consistently high (up to 83% yield of **5a**), highlighting the robust stability and recyclability of CNNs-3. The enduring catalytic performance was corroborated by XRD and FTIR analysis, revealing negligible structural changes in CNNs-3 before and after ten runs, affirming its stability throughout the reaction process. Additionally, a gram-scale reaction with 110 mmol of **4a** (27.5 g) and 55 mmol of **2a** (3.96 g) was conducted to reinforce its practicality (Figure 3b). To ensure uniform light penetration over the reaction mixture and prevent blockages caused by heterogeneous catalysis, a high-speed circulated-flow synthesis using tubular reactor was conducted at a flow rate of 190 mL/min.<sup>[34]</sup> Notably, the reaction yield reached 68% in just 2 hours and eventually up to 96% (12.7 g) in 10 hours. The high efficiency of circulated-flow reactions not only confirms practicality of our protocol but also emphasizes its potential for future industrial application.

### Mechanistic Investigations and Proposed Mechanism

To investigate the reaction mechanism, a series of control experiments were conducted for the aminodifluoroalkylation reaction (Figure 4a). Firstly, adding the commonly used radical inhibitors, such as 2,2,6,6-tetramethylpiperidinyloxy (TEMPO), 1,4-dinitrobenzene, and butylated hydroxytoluene (BHT), resulted in no detection of the corresponding product **5a** under standard conditions, suggesting involvement of radical intermediates. Next, when NaOAc was used in the place of the bulky base LiO<sup>t</sup>Bu, an 82% yield of product **5u** was isolated from the reaction mixture, supporting for the formation of carbocation at the  $\alpha$ -position to the oxygen atom. Furthermore, this cation-trapping experiment also indicates that a strong base is required to deprotonate the amide proton for the lactamization. The necessities of light were further supported by the light on/off experiment with the arylsulfonylation reaction, where no reaction occurred in the absence of light. Additionally, Stern-Volmer quenching experiments between CNNs-3 and **4a** indicated that **4a** could act as a quencher within a reductive quenching cycle (see SI for similar studies with **1a** and Togni reagent **6**). The quantum yields were determined to be 0.32, 0.31, and 0.20 for the arylsulfonylation, aminodifluoroalkylation and oxytrifluoromethylation reactions, respectively. These results provided compelling evidence for the photocatalyzed radical pathway with the CNNs-3, including arylsulfonylation, aminodifluoroalkylation, and oxytrifluoromethylation reactions.

Based on the mechanistic investigations and previous studies, plausible reaction mechanisms are outlined in Figure 4b. Photoexcited electron-hole pairs on the surface of CNNs-3 act as redox centers and initiate the reaction by generation of radicals (R<sup>•</sup>) from the corresponding sulfonyl chlorides **1a** ( $E_{\text{red}} = -1.36$  V vs. SCE), 2-bromo-2,2-difluoro-*N*-arylacetamides **4a** ( $E_{\text{red}} = -1.09$  V vs. SCE) or Togni reagent **6** ( $E_{\text{red}} = -1.25$  V vs. SCE) at the conduction band (CB). The generated radicals (R<sup>•</sup>) subsequently added to the alkene substrates to form the radical intermediate **I**. Subsequent single-electron oxidation of the radical intermediate **I** at the valence band (VB) of CNNs-3 leads to the formation of carbocation intermediate **II**. Depending on the reaction conditions, the carbocation intermediate **II** could undergo either deprotonation in the presence of a base to form the arylsulfonylation products, or nucleophilic attack in the



presence of nucleophiles to afford the aminodifluoroalkylation products (with the amide nitrogen as the nucleophile), or the oxytrifluoromethylation with the carboxylate counterpart of Togni reagent as the nucleophile.

## Conclusions

In summary, we developed an engineered polymeric carbon nitride nanosheet (CNNs-3) as a promising class of metal-free semiconductor photocatalysts, easily prepared from cheap and readily available starting materials via several rounds of calcination under air. The excellent catalytic efficiency of CNNs-3 can be attributed to its augmented specific surface area, enlarged band gap, and the enrichment of vacancies. Specifically, the vacancies in CNNs-3 effectively capture electrons and prevent their recombination with holes, thereby significantly enhancing the electron-hole separation efficiency, which is a critical factor determining their catalytic performance. Our protocol, operating under mild conditions, demonstrates good functional group tolerance and high practicality in diverse functionalization of electron-rich alkenes, including arylsulfonation, aminodifluoroalkylation and oxytrifluoromethylation. The observed recyclability of CNNs-3 and its exceptional performance in large-scale flow synthesis suggest promising avenues for its utilization in an industrial setting and inspire further advances in the development of green and sustainable heterogeneous photocatalysis.

## Acknowledgements

We are grateful for the financial support provided by National Research Foundation, the Prime Minister's Office of Singapore under its NRF-CRP Program (NRF-CRP29-2022-0004, NRF-CRP25-2020RS-0002), A\*STAR MTC-IRG grant (M22K2c0082), National Natural Science Foundation of China (22061044, 22371200, 22309032), Yunnan Revitalization Talent Support Program (Young Talent Project), Natural Science Foundation for Excellent Youth of Anhui Education Department, China (2022AH030056), Anhui Province Action Plan for Cultivating Young and Middle aged Teachers Excellent Young Teacher Cultivation Project (YQYB2023007), and Independent Research Project of Key Laboratory of Green and Precise Synthetic Chemistry and Applications (KLGPSA202202, Huaibei Normal University). We also thank Dr. Hwee Ting Ang for her assistance in writing the manuscript.

## Conflict of Interest

The authors declare no conflict of interest.

## Data Availability Statement

The data that support the findings of this study are available in the supplementary material of this article.

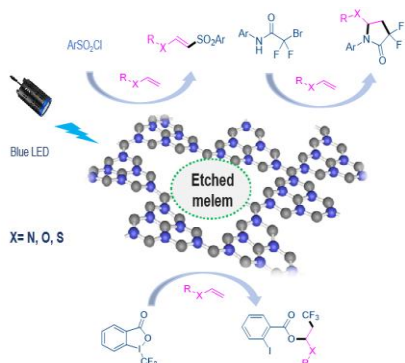
**Keywords:** photocatalytic • polymeric carbon nitride • heterogeneous catalysis • electronic-rich alkene • circulated-flow

- [1] a) N. L. Reed, T. P. Yoon, *Chem. Soc. Rev.* **2021**, *50*, 2954-2967; b) X.-Y. Yu, J.-R. Chen, W.-J. Xiao, *Chem. Rev.* **2021**, *121*, 506-561; c) R. Cannalire, S. Pelliccia, L. Sancineto, E. Novellino, G. C. Tron, M. Giustiniano, *Chem. Soc. Rev.* **2021**, *50*, 766-897; d) B. Qiao, Z. Jiang, *ChemPhotoChem* **2018**, *2*, 703-714.
- [2] a) W. Shang, Y. Li, H. Huang, F. Lai, M. B. J. Roeffaers, B. Weng, *ACS Catal.* **2021**, *11*, 4613-4632; b) B. Su, Z.-C. Cao, Z.-J. Shi, *Acc. Chem. Res.* **2015**, *48*, 886-896; c) D. A. Nicewicz, T. M. Nguyen, *ACS Catal.* **2014**, *4*, 355-360.
- [3] a) S. Vázquez-Céspedes, R. C. Betori, M. A. Cismesia, J. K. Kirsch, Q. Yang, *Org. Process Res. Dev.* **2021**, *25*, 740-753; b) Y. Hu, P. Zhang, J. Du, C. Kim, S. Han, W. Choi, *ACS Catal.* **2021**, *11*, 14941-14955; c) J. Xiao, X. Liu, L. Pan, C. Shi, X. Zhang, J.-J. Zou, *ACS Catal.* **2020**, *10*, 12256-12283; d) I. Ghosh, J. Khamrai, A. Savateev, N. Shlapakov, M. Antonietti, B. König, *Science* **2019**, *365*, 360-366; e) Y. Cai, Y. Tang, L. Fan, Q. Lefebvre, H. Hou, M. Rueping, *ACS Catal.* **2018**, *8*, 9471-9476; f) J. T. Grant, C. A. Carrero, F. Goeltl, J. Venegas, P. Mueller, S. P. Burt, S. E. Specht, W. P. Mcdermott, A. Chieregato, I. Hermans, *Science* **2016**, *354*, 1570-1573; g) J. Chen, J. Cen, X. Xu, X. Li, *Catal. Sci. Technol.* **2016**, *6*, 349-362; h) T. Tsubogo, H. Oyamada, S. Kobayashi, *Nature* **2015**, *520*, 329-332.
- [4] a) K. Bischoff, *Reproductive and Developmental Toxicology, 3rd Edition* **2022**, 503-511; b) F. K. Kessler, Y. Zheng, D. Schwarz, C. Merschjann, W. Schnick, X. Wang, M. J. Bojdys, *Nat. Rev. Mater.* **2017**, *2*, 17030.
- [5] a) S. Yin, X. Zhao, E. Jiang, Y. Yan, P. Zhou, P. Huo, *Energy Environ. Sci.* **2022**, *15*, 1556-1562; b) S. Mazzanti, G. Manfredi, A. J. Barker, M. Antonietti, A. Savateev, P. Giusto, *ACS Catal.* **2021**, *11*, 11109-11116; c) L. Su, P. Wang, X. Ma, J. Wang, S. Zhan, *Angew. Chem. Int. Ed.* **2021**, *60*, 21261-21266; d) H. Chen, H. Shuang, W. Lin, X. Li, Z. Zhang, J. Li, J. Fu, *ACS Catal.* **2021**, *11*, 6193-6199; e) S. Gisbertz, S. Reischauer, B. Pieber, *Nat. Catal.* **2020**, *3*, 611-620; f) A. J. Rieth, Y. Qin, B. C. M. Martindale, D. G. Nocera, *J. Am. Chem. Soc.* **2021**, *143*, 4646-4652; g) A. Vijeta, C. Casadevall, S. Roy, E. Reisner, *Angew. Chem. Int. Ed.* **2021**, *60*, 8494-8499; h) G. Filippini, F. Longobardo, L. Forster, A. Criado, G. D. Carmine, L. Nasi, C. D'Agostino, M. Melchionna, P. Fornasiero, M. Prato, *Sci. Adv.* **2020**, *6*, eabc9923; i) V. W.-H. Lau, I. Moudrakovski, T. Botari, S. Weinberger, M. B. Mesch, V. Duppel, J. Senker, V. Blum, B. V. Lotsch, *Nat. Commun.* **2016**, *7*, 12165.
- [6] a) C. Rosso, G. Filippini, A. Criado, M. Melchionna, P. Fornasiero, M. Prato, *ACS Nano* **2021**, *15*, 3621-3630; b) A. Thomas, A. Fischer, F. Goettmann, M. Antonietti, J.-O. Müller, R. Schlögl, J. M. Carlsson, *J. Mater. Chem.* **2008**, *18*, 4893-4908.
- [7] Q. Liu, H. Cao, W. Xu, J. Li, Q. Zhou, W. Tao, H. Zhu, X. Cao, L. Zhong, J. Lu, X. Peng, J. Wu, *Cell Rep. Phys. Sci.* **2021**, *2*, 100491.
- [8] a) Z. Wen, T. Wan, A. Vijeta, C. Casadevall, L. Buglioni, E. Reisner, T. Noël, *ChemSusChem* **2021**, *14*, 5265-5270; b) C. Yang, R. Li, K. A. I. Zhang, W. Lin, K. Landfester, X. Wang, *Nat. Commun.* **2020**, *11*, 1239; c) B. Pieber, M. Shalom, M. Antonietti, P. H. Seeberger, K. Gilmore, *Angew. Chem., Int. Ed.* **2018**, *57*, 9976-9979.

- [9] a) M. M. Heravi, V. Zadsirjan, *Recent Applications of Selected Name Reactions in the Total Synthesis of Alkaloids*, **2021**, 107-152; b) T. Ghosh, *ChemistrySelect* **2019**, *4*, 4747-4755; c) W. Carruthers, I. Coldham, *Modern Methods of Organic Synthesis*, **2012**, 315-369; d) K. C. Nicolaou, P. G. Bulger, D. Sarlah, *Angew. Chem. Int. Ed.* **2005**, *44*, 4442-4489; e) A. B. Dounay, L. E. Overman, *Chem. Rev.* **2003**, *103*, 2945-2964.
- [10] a) J. Han, R. He, C. Wang, *Chem Catal.* **2023**, *3*, 100690; b) D. Fiorito, S. Scaringi, C. Mazet, *Chem. Soc. Rev.* **2021**, *50*, 1391-1406; c) D. Kurandina, P. Chuentragool, V. Gevorgyan, *Synthesis* **2019**, *51*, 985-1005; d) J. V. Obligacion, P. J. Chirik, *Nature Reviews Chemistry* **2018**, *2*, 15-34; e) Z. Dong, Z. Ren, S. J. Thompson, Y. Xu, G. Dong, *Chem. Rev.* **2017**, *117*, 9333-9403; f) D. M. Cartney, P. J. Guiry, *Chem. Soc. Rev.* **2011**, *40*, 5122-5150; g) S. Tang, K. Liu, C. Liu, A. Lei, *Chem. Soc. Rev.* **2015**, *44*, 1070-1082; h) L. F. Tietze, H. Ila, H. P. Bell, *Chem. Rev.* **2004**, *104*, 3453-3516; i) I. P. Beletskaya, A. V. Cheprakov, *Chem. Rev.* **2000**, *100*, 3009-3066; j) W. Cabri, I. Candiani, *Acc. Chem. Res.* **1995**, *28*, 2-7.
- [11] a) X. Hu, I. Cheng-Sánchez, W. Kong, G. A. Molander, C. Nevado, *Nat. Catal.* **2024**, *7*, 655-665; b) J. Majhi, R. K. Dhungana, Á. Rentería-Gómez, M. Sharique, L. Li, W. Dong, O. Gutierrez, G. A. Molander, *J. Am. Chem. Soc.* **2022**, *144*, 34, 15871-15878; c) H.-Y. Tu, F. Wang, L.-P. Huo, Y.-B. Li, S.-Q. Zhu, X. Zhao, H. Li, F.-L. Qing, L. Chu, *J. Am. Chem. Soc.* **2020**, *142*, 9604-9611; d) C. K. Prier, D. A. Rankic, D. W. C. MacMillan, *Chem. Rev.* **2013**, *113*, 5322-5363; e) J. M. R. Narayanam, C. R. J. Stephenson, *Chem. Soc. Rev.* **2011**, *40*, 102-113; f) T. P. Yoon, M. A. Ischay, J. Du, *Nat. Chem.* **2010**, *2*, 527-532; g) J. Xuan, W.-J. Xiao, *Angew. Chem. Int. Ed.* **2012**, *51*, 6828-6838.
- [12] a) Y. Liu, H. Liu, X. Liu, Z. Chen, *Catalysts* **2023**, *13*, 1056; b) T. Koike, M. Akita, *Chem* **2018**, *4*, 409-437.
- [13] F. Zhou, M. Li, H. Jiang, W. Wu, *Adv. Synth. Catal.* **2021**, *363*, 4841-4855.
- [14] a) M. S. Spektor, D. Kellen, K. C. Klauer, *Cognition* **2022**, *225*, 105164; b) C. Tantardini, A. R. Oganov, *Nat. Commun.* **2021**, *12*, 2087.
- [15] D. H.R. Barton, M. A. Csiba, J. Cs. Jaszberenyi, *Tetrahedron Lett.* **1994**, *35*, 2869-2872.
- [16] Y. Tanaka, S. Kubosaki, K. Osaka, M. Yamawaki, T. Morita, Y. Yoshimi, *J. Org. Chem.* **2018**, *83*, 13625-13635.
- [17] H. Wang, P. Bellotti, X. Zhang, T. O. Paulisch, F. Glorius, *Chem* **2021**, *7*, 3412-3424.
- [18] H. Jiang, X. Yu, C. G. Daniliuc, A. Studer, *Angew. Chem. Int. Ed.* **2021**, *60*, 14399-14404.
- [19] J.-W. Wang, Y. Li, W. Nie, Z. Chang, Z.-A. Yu, Y.-F. Zhao, X. Lu, Y. Fu, *Nat. Commun.* **2021**, *12*, 1313.
- [20] a) X.-Y. Bai, W.-W. Zhang, Q. Li, B.-J. Li, *J. Am. Chem. Soc.* **2018**, *140*, 506-514; b) X.-Y. Bai, Z.-X. Wang, B.-J. Li, *Angew. Chem. Int. Ed.* **2016**, *55*, 9007-9011.
- [21] a) D. Bouchet, T. Varlet, G. Masson, *Acc. Chem. Res.* **2022**, *55*, 3265-283; b) R. Sun, X. Yang, Y. Ge, J. Song, X. Zheng, M. Yuan, R. Li, H. Chen, H. Fu, *ACS Catal.* **2021**, *11*, 11762-11773; c) R. Abrams, J. Clayden, *Angew. Chem. Int. Ed.* **2020**, *59*, 11600-11606; d) W. Fan, S. Yamago, *Angew. Chem. Int. Ed.* **2019**, *58*, 7113-7116; e) A. Alix, C. Lalli, P. Retailleau, G. Masson, *J. Am. Chem. Soc.* **2012**, *134*, 10389-10392; f) C. Feng, T.-P. Loh, *Chem. Sci.* **2012**, *3*, 3458-3462; g) K. Gopalaiah, H. B. Kagan, *Chem. Rev.* **2011**, *111*, 4599-4657; h) R. Matsubara, S. Kobayashi, *Acc. Chem. Res.* **2008**, *41*, 292-301.
- [22] H. Yu, R. Shi, Y. Zhao, T. Bian, Y. Zhao, C. Zhou, G. I. N. Waterhouse, L.-Z. Wu, C.-H. Tung, T. Zhang, *Adv. Mater.* **2017**, *29*, 1605148.
- [23] J. Ran, T. Y. Ma, G. Gao, X.-W. Du, S. Z. Qiao, *Energy Environ. Sci.* **2015**, *8*, 3708-3717.
- [24] P. Niu, L. Zhang, G. Liu, H.-M. Cheng, *Adv. Funct. Mater.* **2012**, *22*, 4763-4770.
- [25] Q. Liang, Z. Li, Z.-H. Huang, F. Kang, Q.-H. Yang, *Adv. Funct. Mater.* **2015**, *25*, 6885-6892.
- [26] S. B. Yang, Y. J. Gong, J. S. Zhang, L. Zhan, L. L. Ma, Z. Y. Fang, R. Vajtai, X. C. Wang, P. M. Ajayan, *Adv. Mater.* **2013**, *25*, 2452-2457.
- [27] H. Yaghoubi, Z. Li, Y. Chen, H.T. Ngo, V.R. Bhethanabotla, B. Joseph, S. Ma, R. Schlaf, A. Takshi, *ACS Catal.* **2015**, *5*, 327-335.
- [28] D. Zhao, C.-L. Dong, B. Wang, C. Chen, Y.-C. Huang, Z. Diao, S. Li, L. Guo, S. Shen, *Adv. Mater.* **2019**, *31*, 1903545.
- [29] Y. Xiao, G. Tian, W. Li, Y. Xie, B. Jiang, C. Tian, D. Zhao, H. Fu, *J. Am. Chem. Soc.* **2019**, *141*, 2508-2515.
- [30] a) Y. Deng, L. Tang, G. Zeng, Z. Zhu, M. Yan, Y. Zhou, J. Wang, Y. Liu, J. Wang, *Appl. Catal. B*, **2017**, *203*, 343-354; b) Y. Ma, E. Liu, X. Hu, C. Tang, J. Wan, J. Li, J. Fan, *Appl. Surf. Sci.* **2015**, *358*, 246-251; c) X. Zhang, X. Xie, H. Wang, J. Zhang, B. Pan and Y. Xie, *J. Am. Chem. Soc.* **2013**, *135*, 18-21.
- [31] J. Fu, K. Liu, K. Jiang, H. Li, P. An, W. Li, N. Zhang, H. Li, X. Xu, H. Zhou, D. Tang, X. Wang, X. Qiu, M. Liu, *Adv. Sci.* **2019**, *6*, 1900796.
- [32] a) X. Li, Y. Sun, J. Xu, Y. Shao, J. Wu, X. Xu, Y. Pan, H. Ju, J. Zhu, Y. Xie, *Nat. Energy.* **2019**, *4*, 690-699; b) D. Zhao, C.-L. Dong, B. Wang, C. Chen, Y.-C. Huang, Z. Diao, S. Li, L. Guo, S. Shen, *Adv. Mater.* **2019**, *31*, 1903545.
- [33] H. Egami, M. Sodeoka, *Angew. Chem. Int. Ed.* **2014**, *53*, 2-17.
- [34] C. Liu, L. Song, Q. Liu, W. Chen, J. Xu, M. Wang, Y. Zhang, T., W. Tan, Z. Lei, L. Cheng, S. A. Khan, J. Wu, *Org. Process Res. Dev.* **2024**, *28*, 1964-1970.

## RESEARCH ARTICLE

WILEY-VCH

Entry for the Table of Contents  
RESEARCH ARTICLE

Youqing Yang,<sup>‡</sup> [a,b] Jiwei Shi,<sup>‡</sup> [b,c]  
Chenguang Liu,<sup>[b]</sup> Qiong Liu,<sup>[b,d]</sup> Jian  
Yang,<sup>[b]</sup> Xiaogang Tong,<sup>\*,[b,e]</sup> Jiong Lu,<sup>\*,[b]</sup>  
and Jie Wu<sup>\*,[b]</sup>

Page No. – Page No.

Engineered Polymeric Carbon Nitride  
for Photocatalytic Diverse  
Functionalization of Electronic-Rich  
Alkenes

Vacancy engineered polymeric carbon nitride nanosheets were developed as highly efficient heterogeneous photocatalysts for the diverse functionalization of electronic-rich alkenes.